

## Phase stabilities of $\text{MgCO}_3$ and $\text{MgCO}_3\text{-II}$ studied by Raman spectroscopy, x-ray diffraction, and density functional theory calculations

Jannes Binck <sup>1,\*</sup>, Lkhamsuren Bayarjargal,<sup>1</sup> Sergey S. Lobanov,<sup>2</sup> Wolfgang Morgenroth <sup>1</sup>, Rita Luchitskaia,<sup>1</sup> Chris J. Pickard,<sup>3,4</sup> Victor Milman <sup>5</sup>, Keith Refson <sup>6,7</sup>, Dominik B. Jochym <sup>8</sup>, Peter Byrne,<sup>9</sup> and Björn Winkler<sup>1</sup>

<sup>1</sup>Institut für Geowissenschaften, Goethe-Universität Frankfurt, Altenhöferallee 1, 60438 Frankfurt am Main, Germany

<sup>2</sup>Deutsches GeoForschungsZentrum GFZ, Telegrafenberg, Building D, 14473 Potsdam, Germany

<sup>3</sup>Department of Materials Science & Metallurgy, University of Cambridge, 27 Charles Babbage Road, Cambridge CB3 0FS, United Kingdom

<sup>4</sup>Advanced Institute for Materials Research, Tohoku University 2-1-1 Katahira, Aoba, Sendai, 980-8577, Japan

<sup>5</sup>BIOVIA Dassault Systèmes, 334 Science Park, Cambridge CB4 0WN, United Kingdom

<sup>6</sup>Department of Physics, Royal Holloway, University of London Egham, Surrey TW20 0EX, United Kingdom

<sup>7</sup>ISIS Facility, Rutherford Appleton Laboratory, Chilton, Didcot, Oxfordshire, OX11 0QX, United Kingdom

<sup>8</sup>Scientific Computing Department, Rutherford Appleton Laboratory, Chilton, Didcot, Oxfordshire OX11 0QX, United Kingdom

<sup>9</sup>Department of Physics, University of York, Heslington YO10 5DD, United Kingdom



(Received 21 January 2020; revised manuscript received 30 March 2020; accepted 7 April 2020; published 4 May 2020)

Carbonates are the major hosts of carbon on Earth's surface and their fate during subduction needs to be known to understand the deep carbon cycle. Magnesite ( $\text{MgCO}_3$ ) is thought to be an important phase participating in deep Earth processes, but its phase stability is still a matter of debate for the conditions prevalent in the lowest part of the mantle and at the core mantle boundary. Here, we have studied the phase relations and stabilities of  $\text{MgCO}_3$  at these  $P, T$  conditions, using Raman spectroscopy at high pressures ( $\sim 148$  GPa) and after heating to high temperatures ( $\sim 3600$  K) in laser-heated diamond anvil cell experiments. The experimental Raman experiments were supplemented by x-ray powder diffraction data, obtained at a pressure of 110 GPa. Density-functional-theory-based model calculations were used to compute Raman spectra for several  $\text{MgCO}_3$  high-pressure polymorphs, thus allowing an unambiguous assignment of Raman modes. By combining the experimental observations with the density-functional-theory results, we constrain the phase stability field of  $\text{MgCO}_3$  with respect to the high-pressure polymorph,  $\text{MgCO}_3\text{-II}$ . We further confirm that Fe-free  $\text{MgCO}_3\text{-II}$  is a tetracarbonate with monoclinic symmetry (space group  $C2/m$ ), which is stable over the entire  $P, T$  range of the Earth's lowermost mantle geotherm.

DOI: [10.1103/PhysRevMaterials.4.055001](https://doi.org/10.1103/PhysRevMaterials.4.055001)

### I. INTRODUCTION

The Earth's mantle is believed to experience a carbon influx on the order of teragrams per year, due to the subduction of oceanic lithosphere [1,2]. Carbonate minerals are considered to constitute the major carbon source during subduction processes [2–6]. In the mantle, decomposition reactions of carbonates and reactions with silicates are thought to lead to the formation of other carbon-containing phases [7–10]. As silicates can only incorporate very minor amounts of carbon at mantle conditions [11,12], the most prevalent carbon-bearing phases are believed to be diamond [13], high  $P, T$  phases of  $\text{CO}_2$  [14], or metal carbides [15,16]. However, carbonates may survive in the Earth's mantle in cold oxidized subducting slabs [17,18], some of which might penetrate into the lowermost mantle [19]. This model is supported by the presence of carbonate inclusions [ $\text{CaCO}_3$ ,  $\text{MgCO}_3$ ,  $\text{CaMg}(\text{CO}_3)_2$ ] in mantle xenoliths and in superdeep diamonds [20–25].

Magnesite ( $\text{MgCO}_3$ ) is thought to be stable under  $P, T$  conditions of the Earth's mantle [9,26,27]. While other carbonates undergo several phase transitions [e.g., calcite ( $\text{CaCO}_3$ ) [28], or decompose at  $P, T$ -conditions of the Earth's mantle (e.g., dolomite [ $\text{CaMg}(\text{CO}_3)_2$ ] and siderite ( $\text{FeCO}_3$ ) [29,30], magnesite remains stable up to at least 80 GPa and 3000 K [26,31,32]. Studies of reactions of  $\text{MgCO}_3$  with  $\text{SiO}_2$  implied that high-pressure, high-temperature polymorphs of  $\text{MgCO}_3$  might coexist with silicates in supercold slabs in the lower mantle [9]. Model calculations of reactions of  $\text{MgCO}_3/\text{CaCO}_3$  with  $\text{MgO}/\text{MgSiO}_3$  under  $P, T$  conditions of the Earth's lower mantle imply the possible existence of oxidized carbon in the form of  $\text{MgCO}_3$  in the absence of iron [33,34].

Based on *in situ* powder x-ray diffraction, Isshiki *et al.* [26] showed that magnesite ( $R\bar{3}c$ ,  $Z = 6$ ) undergoes a phase transition to magnesite-II at deep lower mantle conditions ( $> 115$  GPa and 2200 K). Shortly after these findings, density-functional-theory (DFT)-based predictions reported the possibility of the existence of very high-pressure (e.g., at pressures  $> 80$  GPa) carbonate structures that are characterized by  $sp^3$ -hybridized bonding environments within  $\text{CO}_4^{4-}$  tetrahedrons

\*binck@kristall.uni-frankfurt.de

instead of triangular  $sp^2$ -hybridized  $\text{CO}_3^{3-}$  groups [35–39]. Within the last decade, the existence of so-called tetracarboxates has been confirmed by several experimental studies [30,40–45].

Several theoretical structures have been reported for  $sp^3$ - $\text{MgCO}_3$  polymorphs [35,38,39]. Combined results from DFT and x-ray powder diffraction suggested a  $\text{MgCO}_3$  structure with space group  $C2/m$  and  $Z = 12$  formula units to be the most stable phase at pressures between 82–138 GPa [38]. However, a comparison of powder x-ray diffraction data of the  $C2/m$ -phase with powder patterns published by Isshiki *et al.* [26] gave an unsatisfactory match. Further experimental evidence for the formation of the  $C2/m$  phase around  $\sim 82$  GPa was given by Boulard *et al.* [40] and Maeda *et al.* [9]. However, their data analyses relied on Le Bail fits only. While x-ray powder diffraction data were fitted with the  $C2/m$  phase between 85–152 GPa in the study by Maeda *et al.* [9], a lower symmetric structure with space group  $P2_1/c$  was proposed to be better suited for fitting x-ray diffraction patterns by Boulard *et al.* [40] at 82 GPa.

Using a sample with an initial composition of  $\text{Fe}_{0.15}\text{Mg}_{0.85}\text{CO}_3$  at ambient conditions, Chariton *et al.* [46] have been able to solve the crystal structure of  $\text{Fe}_{0.4}\text{Mg}_{2.6}\text{C}_3\text{O}_9$  at 98 GPa and after heating to 2500 K from single-crystal data. This structure was shown to be identical to the  $C2/m$  phase proposed by Oganov *et al.* [38].

While the existence of the  $C2/m$  phase now seems to be established for pressures  $< 100$  GPa and temperatures  $< 2500$  K [46], significant gaps and inconsistencies remain in our understanding of the high  $P, T$  behavior of Fe-free  $\text{MgCO}_3$  [9,26,38,39]. Currently, all experimental data above 100 GPa rely on poorly constrained indexing of x-ray powder diffraction patterns [9,26,38], while theoretical calculations suggest several possible low-energy structures [35,38,39]. The strength of vibrational spectroscopy for the detection of high-pressure, high-temperature phases in the diamond anvil cell (DAC) has recently been exploited for high-pressure studies on different carbonates [28,29,42,45,47–49]. Raman spectroscopy is a very sensitive method, which may provide additional structural information for the particular high-pressure, high-temperature polymorphs of  $\text{MgCO}_3$  thus complementing previous x-ray diffraction studies. However, studies that have been employing Raman spectroscopy on  $\text{MgCO}_3$  are limited to pressures  $< 55$  GPa [32,47,50,51].

In this paper, we have investigated the  $\text{MgCO}_3$  system in the entire pressure and temperature range reaching to the uppermost part of the Earth's outer core corresponding to pressures up to  $\sim 148$  GPa and temperatures up to  $\sim 3600$  K. We combined Raman spectroscopy in the laser-heated DAC with DFT-based model calculations. Supplementary x-ray powder diffraction data were obtained at high pressures, which support our observations further.

## II. METHODS

Syntheses, preparations of experiments, sample characterizations at ambient conditions, as well as Raman spectroscopy in the LH-DAC have been carried out at the Institute of Geosciences at the Goethe Universität Frankfurt, Germany. The high pressure x-ray diffraction experiments have been

carried out at P02.2 at PETRA III (DESY) in Hamburg, Germany.

### A. Synthesis

Single crystals of magnesite were synthesized according to the method described by Ni *et al.* [52]. All chemicals (magnesium acetate tetrahydrate, hexamethylenetetramine, and sodium sulfate) were analytical grade reagents purchased from Merck KGaA (Darmstadt) and used as received without further purification. 3 mmol magnesium acetate, 3 mmol hexamethylenetetramine, and 0.6 g sodium sulfate were dissolved in 40 ml bidistilled water. After stirring for 30 min, the obtained transparent solution was transferred into a 60 ml Teflon cup, which was filled to 60% of its volume. Subsequently, the cup was put into a stainless steel autoclave and sealed tightly. After reaction at  $160^\circ\text{C}$  for 48 h, the autoclave was slowly cooled down ( $160$ – $100^\circ\text{C}$  in 48 h, then  $100$ – $25^\circ\text{C}$  in 12 h). The precipitate was filtered under vacuum, washed with distilled water repeatedly, and dried at  $60^\circ\text{C}$  in an oven. The slow cooling allowed us to grow crystals with edge lengths up to  $60\ \mu\text{m}$ .

### B. Characterization

The phase purity of the synthesized batch of single crystals has been characterized at ambient conditions by x-ray powder diffraction. Therefore, we separated the majority of single crystals from the synthesized batch and grounded a fine sample powder in an agate mortar. The grounded sample powder was measured using an X'Pert Pro diffractometer equipped with a linear position-sensitive detector from PANalytical (PIXcel<sup>3D</sup>) and a Johansson monochromator (Ge 111) using  $\text{CuK}\alpha_1$  radiation ( $\lambda = 1.5418\ \text{\AA}$ ) generated at 40 kV and 30 mA. A Rietveld refinement was carried out using the GSAS-II software [53] and a reported structure of magnesite [54] as a starting model (see Supplemental Material [55]). The refined lattice parameters were  $a = b = 4.6375(1)\ \text{\AA}$ ,  $c = 15.0268(2)\ \text{\AA}$ , and  $V = 279.876(1)\ \text{\AA}^3$ , which are consistent with the parameters of the established structure of magnesite [54]. Additionally, Raman spectroscopy was carried out at ambient conditions on single crystals. The spectra confirmed the excellent sample quality (Fig. 1).

### C. Preparation of high-pressure, high-temperature experiments

High-pressure, high-temperature experiments were carried out using Boehler-Almax DACs [56]. Type Ia and IIa diamonds with low birefringence and ultralow fluorescence having either regular culets (200-, 250-, and 350- $\mu\text{m}$  diameter), or beveled culets ( $9^\circ$  bevel, 100- $\mu\text{m}$  inner, and 220- $\mu\text{m}$  outer diameter) were inserted in tungsten carbide seats. The opening angles of the cells were  $48^\circ$  or  $70^\circ$ . Depending on the culet size, sample chambers of 45–160  $\mu\text{m}$  in diameter were laser drilled in Re gaskets preindented to  $\sim 40\ \mu\text{m}$ . Before loading, the sample material was dried at  $150^\circ\text{C}$  for 24 h in an oven. Immediately after drying, three DACs were loaded with single crystals and one cell with a compacted powder. The single crystals had edge lengths of  $\sim 15\ \mu\text{m}$ . All cells were loaded with a ruby pressure marker. Neon served as a pressure transmitting medium for the single crystal cells,

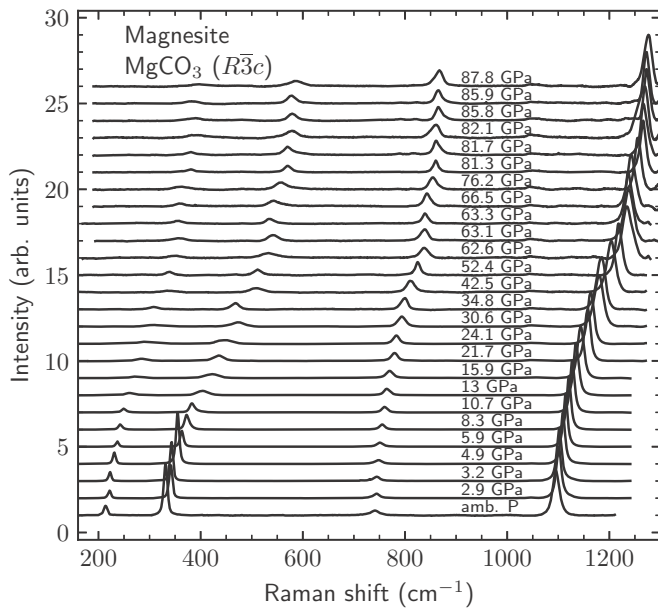


FIG. 1. High-pressure Raman spectra of  $\text{MgCO}_3$  (magnesite) from ambient pressure to  $\sim 88$  GPa as obtained for a single run. For most of the pressure steps between 15.9 and 82.1 GPa, the crystal was slightly annealed at temperatures  $< 1000$  K. All Raman measurements were conducted after quenching the sample to ambient temperature.

which was loaded by a custom-built gas loading system. To obtain x-ray powder diffraction data without any interference by the pressure-transmitting medium, no neon gas was used for the DAC loaded with the compacted powder sample. No further thermal insulation was added to the loadings to prevent possible chemical reactions.

#### D. Raman spectroscopy in the LH-DAC

Raman spectra were measured in 0.5–4 GPa steps upon compression and decompression covering a range between ambient pressure and  $\sim 148$  GPa. A frequency-doubled 532.14 nm Nd:YAG Oxxius laser (LCX-532S) was focused on the sample with a spot size of 6  $\mu\text{m}$ . Spectra were collected in backscattering geometry, using a grating spectrometer (Acton, SP-2356) equipped with a CCD detector (Pixis 256E) and a microscope objective (Mitutoyo). The spectral resolution of the spectrometer is  $3\text{ cm}^{-1}$  [28]. The laser power was set to 430 mW and spectra were collected for 50 s in a frequency window of  $100\text{--}1500\text{ cm}^{-1}$ , using a grating of 1800 grooves/mm. The estimated laser power on the sample was around  $\sim 350$  mW. For measurements up to 95 GPa, the pressure was determined before and after the Raman measurement, using the ruby reference scales for non-[57] and quasihydrostatic conditions [58]. Pressures were further determined for  $P \geq 45$  GPa using the diamond edge reference scale [59]. For  $P > 95$  GPa, only the diamond edge reference scale was employed. According to Dewaele *et al.* [60], the uncertainty in pressures determined by Mao *et al.* [57] increases from 0.05 GPa at 1 GPa up to 2 GPa at 150 GPa. The accuracy of our pressure determination by the ruby and diamond reference scales was  $\leq 2$  GPa, while

pressure gradients may have caused uncertainties up to 4 GPa during and after laser heating.

The sample was heated from both sides with a pulsed  $\text{CO}_2$  laser (Diamond K-250 from Coherent,  $\lambda = 10.6\ \mu\text{m}$ ) [28]. For the spectroradiometric temperature determination, we used the same setup as for the Raman measurements, while the grating was set to 150 grooves/mm. To achieve coupling of the  $\text{CO}_2$  heating laser from both sides of the sample, the laser power was typically set in a range between 1–6 W, depending on the pressure and the loading of the DAC. The heating laser was focused on the sample so the diameter of the heated area was around 25  $\mu\text{m}$ , which nearly covered all of the single crystals. However, due to the poor-to-moderate coupling of the laser with the samples, heating was inhomogeneous. Hence, we moved the heating laser across the sample, while typically heating for about 5 min per position. The position of the Raman laser with respect to the heated areas on the sample was controlled using an optical camera. The thermal emission of the sample, as well as the Raman signal were measured with a spatial resolution of around 5–6  $\mu\text{m}$ , i.e., the areas for the measurements were significantly smaller than the heating spots. The temperatures during laser heating were determined by the two-color pyrometer method, employing Planck and Wien fits [61]. We assume a typical uncertainty associated with radiometric temperature measurements in LH-DACs of  $\sim 10\%$ .

#### E. High-pressure x-ray diffraction

High pressure x-ray powder diffraction measurements have been carried out at the extreme conditions beamline P02.2 at PETRA III (DESY, Hamburg, Germany). X-ray diffraction data were collected for a  $\text{MgCO}_3$  powder sample, which at first was pressurized to 110 GPa in a DAC and temperature quenched after laser heating to  $\sim 2500$  K. The diffraction patterns were acquired using a wavelength of 0.2898 Å, a beam focused to  $8 \times 3\ \mu\text{m}^2$  (full width at half maximum), compound reflective lenses, and a Perkin Elmer XRD 1621 flat-panel detector. A grid of  $5 \times 5$  points with spacings of 2  $\mu\text{m}$  between each point was measured. The DAC was rotated by  $\pm 10^\circ$  with an exposure time of 40 s for every data point collection. The sample-to-detector distance of 402.78 mm and the wavelength were determined employing a  $\text{CeO}_2$  reference sample. The diffraction data were processed with the DIOPTAS software [62]. Rietveld refinements were carried out using the GSAS-II software [53] and the structure model based on an earlier description of the  $C2/m$  phase [38].

#### F. Density functional theory

To obtain theoretical Raman spectra, density functional perturbation theory (DFPT) calculations were performed employing the CASTEP code [63]. The code is an implementation of Kohn-Sham DFT based on a plane-wave-basis set in conjunction with pseudopotentials. The plane-wave-basis set allows us to achieve numerically converged results in a straightforward manner, as the convergence is controlled by a single adjustable parameter, the plane-wave cutoff, which we set to 1020 eV. For calculations for pressures  $< 100$  GPa, the norm-conserving pseudopotentials were generated “on

the fly” from the information provided in the CASTEP data base. These pseudopotentials have been tested extensively for accuracy and transferability [64]. For calculations at pressures >100 GPa, norm-conserving pseudopotentials with smaller core radii were constructed to avoid overlap of ionic cores. The descriptors of these pseudopotentials are given in the Supplemental Material [55]. All calculations employed the GGA-PBE exchange-correlation functional [65]. The Brillouin zone integrals were performed using Monkhorst-Pack grids [66] with spacings between grid points of less than  $0.037 \text{ \AA}^{-1}$ . Geometry optimizations were defined as being converged when the energy change between iterations was  $<0.5 \times 10^{-6} \text{ eV/atom}$ , the maximal residual force was  $<0.01 \text{ eV/\AA}$ , and the maximal residual stress was  $<0.02 \text{ GPa}$ . Phonon frequencies were obtained from DFPT calculations. Raman intensities were computed using DFPT in the  $2n + 1$  theorem approach [67].

### III. RESULTS AND DISCUSSION

#### A. $\text{MgCO}_3$ (magnesite) at high pressures and high temperatures measured by Raman spectroscopy

The characteristic Raman phonon frequencies of  $\text{MgCO}_3$  (magnesite) were measured in four different experimental runs, covering a pressure range between ambient pressure and  $\sim 107 \text{ GPa}$  (Figs. 1 and 2). According to group theory, the following Raman and infrared active modes are expected for magnesite at ambient conditions:  $\Gamma = A_{1g}(\text{R}) + 3A_{2u}(\text{IR}) + 5E_u(\text{IR}) + 4E_g(\text{R})$ . All Raman active modes were observed at ambient conditions. Starting at ambient pressure with a frequency of  $1444 \text{ cm}^{-1}$ , the  $E_g(\nu_3)$  mode is obscured by the first-order Raman mode of the diamond anvils in the DAC experiments. The frequencies of the symmetric stretching mode and the symmetric in-plane bend allow a straightforward identification of the  $\text{CO}_3^{2-}$  groups [50,68,69]. We observed the  $A_{1g}(\nu_1)$  and  $E_g(\nu_4)$  modes up to  $\sim 107 \text{ GPa}$  in a range between  $1095\text{--}1304 \text{ cm}^{-1}$  and  $740\text{--}893 \text{ cm}^{-1}$ , respectively. The two low-frequency  $E_g$  modes ( $\nu = 213$  and  $331 \text{ cm}^{-1}$  at ambient pressure) were observed up to  $45.5 \text{ GPa}$ . At higher pressures, these modes displayed a significant broadening or disappeared completely. A similar behavior for the low-frequency  $E_g$  modes was reported by Williams *et al.* [50] and Gillet [51], who observed the  $213 \text{ cm}^{-1}$  Raman band at pressures between  $13\text{--}20 \text{ GPa}$  and the  $331 \text{ cm}^{-1}$  Raman band up to  $26 \text{ GPa}$ .

We were able to detect all Raman active modes that are observable in a DAC up to  $87.8 \text{ GPa}$  by carefully thermally annealing the single crystal at nearly each pressure step up to  $82 \text{ GPa}$  and measuring the Raman signal after temperature quenching (Fig. 1). The temperatures during the thermal annealing by the laser were estimated to be  $<1000 \text{ K}$ , since no visible thermal radiation was observed. An offset for especially the low-frequency Raman modes may be observed for some of the high-pressure Raman spectra due to the non-hydrostatic pressure on the sample. These effects disappeared after heating was applied and hydrostatic conditions on the sample were increased.

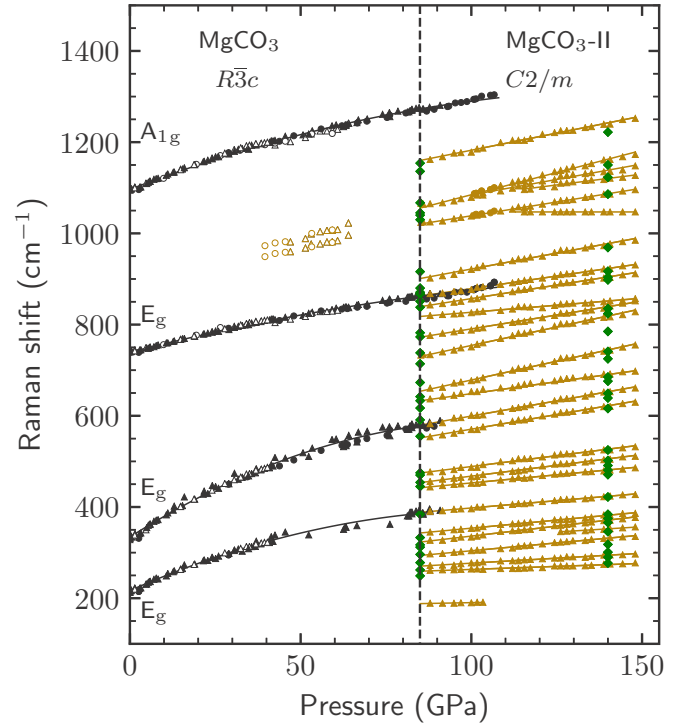


FIG. 2. Pressure dependence of the characteristic Raman modes of magnesite (black symbols) and  $\text{MgCO}_3\text{-II}$  (yellow symbols). Triangles and circles correspond to single crystal and powder samples, respectively. Open symbols correspond to data obtained under cold decompression. DFT-calculated phonon frequencies of  $\text{MgCO}_3\text{-II}$  at  $85$  and  $140 \text{ GPa}$  are shown for comparison (green diamond symbols). The black dashed line marks the phase boundary of the  $\text{MgCO}_3$  polymorphs at  $85 \text{ GPa}$ . Data points were fitted using linear or quadratic fits.

#### B. Phase transition of $\text{MgCO}_3$ (magnesite) to $\text{MgCO}_3\text{-II}$ identified by Raman spectroscopy, XRD, and density functional theory

At  $83 \text{ GPa}$  and after heating to  $\sim 2400 \text{ K}$ , our Raman spectra still indicate the presence of  $\text{MgCO}_3$  (magnesite) at these conditions, while a drastic change in the spectra is observed at around  $85 \text{ GPa}$  and after heating to  $\sim 2000 \text{ K}$ , where new characteristic Raman bands were observed besides those of  $\text{MgCO}_3$  (magnesite) [55]. At  $87.9 \text{ GPa}$  and after heating to maximum temperatures of  $\sim 3100 \text{ K}$ , Raman spectra yielded at least 23 strong intense modes covering a frequency range between  $250$  and  $1250 \text{ cm}^{-1}$  (Fig. 3). These changes are due to a phase transition from  $\text{MgCO}_3$  (magnesite) to a second phase, which we have labeled  $\text{MgCO}_3\text{-II}$  here. We computed the Raman spectra for the monoclinic  $C2/m$  phase [38,46] and for a hypothetical triclinic  $P\bar{1}$  phase [39], which has been suggested to be stable between  $85\text{--}101 \text{ GPa}$ . The experimental Raman spectrum at  $87.9 \text{ GPa}$  can very satisfactorily be explained by a combination of the theoretical Raman spectra of magnesite and the  $C2/m$  phase, while no indication for the  $P\bar{1}$  phase was found (Fig. 3).

We continued measuring Raman spectra up to  $148 \text{ GPa}$  (Figs. 2 and 4). For most of the pressure steps, the sample was heated to maximum temperatures of  $\sim 3600 \text{ K}$  prior to the measurement to achieve a hydrostatic pressure distribution on

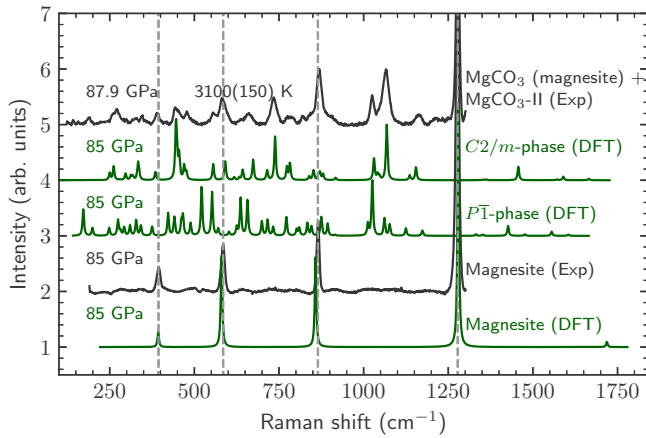


FIG. 3. Experimental Raman spectra of MgCO<sub>3</sub> (magnesite) and a mixture of MgCO<sub>3</sub> (magnesite) and MgCO<sub>3</sub>-II (*C2/m*-phase [38]) are shown in black. DFT-calculated Raman spectra of magnesite, the *C2/m* phase, and the *P* $\bar{1}$  phase [39] are shown in green. DFT frequencies were calculated with a FWHM broadening of 5 cm<sup>-1</sup>. The calculated frequencies were multiplied by a scaling factor of 1.02. The characteristic Raman modes of MgCO<sub>3</sub> (magnesite) at 85 GPa are indicated by dashed grey lines.

the sample. A comparison of theoretical spectra with experimental data at 115 and 140 GPa shows an excellent match of frequencies and intensities (Fig. 5). Characteristic modes of MgCO<sub>3</sub> (magnesite) are no longer observed in the experimental spectrum at these conditions. According to group theory, the irreducible representations of the *C2/m* phase for the Raman and infrared modes are  $\Gamma = 25A_g(R) + 18A_u(IR) + 20B_g(R) + 24B_u(IR)$ . The tetrahedral CO<sub>4</sub><sup>4-</sup> groups of the *C2/m* phase are polymerized and form corner-sharing C<sub>3</sub>O<sub>6</sub><sup>6-</sup> rings [38]. Between 85 and 148 GPa, characteristic vibrations

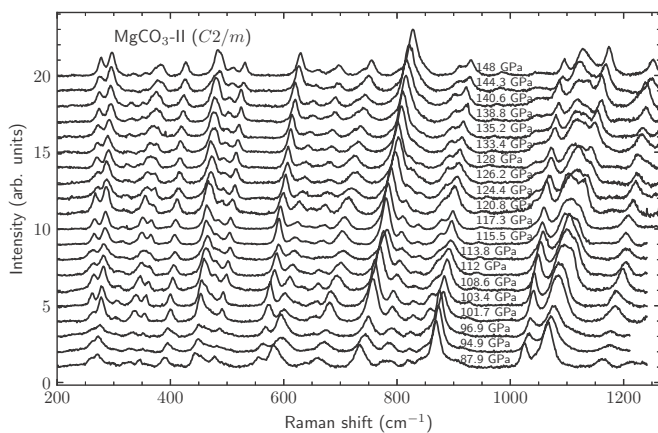


FIG. 4. Raman spectra of MgCO<sub>3</sub>-II (*C2/m*-phase) [38] in a pressure range from 87 to 148 GPa for a single run. For most of the pressure steps, the sample was heated to maximum temperatures between 3000 and 3600 K and measured after quenching to ambient temperature. For the present data, the grating of the Raman spectrometer was centered towards higher Raman shifts, which resulted in obscuration of the CO<sub>3</sub>-stretching mode ( $\nu = 1278$  cm<sup>-1</sup>) by the diamond anvils.

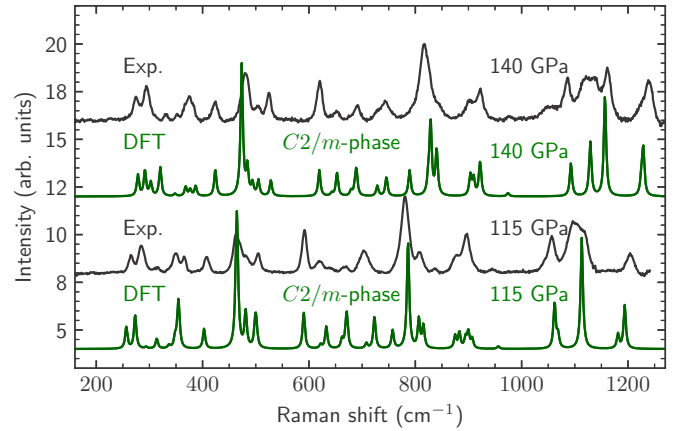


FIG. 5. Comparison between Raman bands of experimental data (black) and theoretical data (green) of MgCO<sub>3</sub>-II (*C2/m* phase [38]) at 115 and 140 GPa. Experimental data have been obtained on the temperature-quenched sample after heating to ~3000 and ~3200 K, respectively. The experimental spectrum reveals the complete transformation of MgCO<sub>3</sub> (magnesite) to MgCO<sub>3</sub>-II at these conditions. DFT frequencies were calculated with a FWHM broadening of 5 cm<sup>-1</sup>. The calculated frequencies were multiplied by a scaling factor of 1.02.

of those rings are frequencies in the ranges 1023–1095 cm<sup>-1</sup>, 1026–1128 cm<sup>-1</sup>, 1050–1146 cm<sup>-1</sup>, and 1065–1173 cm<sup>-1</sup>, respectively. Further characteristic features are the intense A<sub>g</sub> and B<sub>g</sub> modes at 733–781 cm<sup>-1</sup> and 444–463 cm<sup>-1</sup>, respectively. Both modes are due to relative movements between the C<sub>3</sub>O<sub>6</sub><sup>6-</sup> rings and the Mg<sup>2+</sup> cations. Two modes in MgCO<sub>3</sub>-II at 189 cm<sup>-1</sup> ( $\leq 105$  GPa) and 1050 cm<sup>-1</sup> ( $\geq 120$  GPa) have no correspondence in the DFT calculations. The origin of these modes is currently unexplained.

There have been suggestions that the *C2/m* polymorph transforms into another phase at  $P \geq 138$  GPa. For this phase, structures with space group *P2*<sub>1</sub> [38] or *P2*<sub>1</sub>2<sub>1</sub>2<sub>1</sub> [39] have been suggested. Theoretical Raman spectra of the hypothetical *P2*<sub>1</sub> phase [38] at 120 and at 140 GPa were computed and compared to our experimental observations [55]. Although the comparison between experimental and theoretical spectra exhibits some similarities at higher frequencies, significant differences are observed in the lower frequency range. Hence, we conclude that this phase has not been formed in our experiments. Computation of the Raman spectra of the *P2*<sub>1</sub>2<sub>1</sub>2<sub>1</sub> phase [39] was beyond the available computation resources.

Our combined results from Raman spectroscopy and DFT-calculations are supported by synchrotron x-ray powder diffraction measurements, which have been conducted on MgCO<sub>3</sub> powder at 110 GPa and after heating to ~2500 K. We were able to successfully carry out a Rietveld refinement, which allowed the identification of the *C2/m* phase (Fig. 6 and Supplemental Material [55]). Since Rietveld refinements are usually hard to conduct for high-pressure data, especially after heating, intensities of a grid of 25 diffraction images were summed at each particular 2 theta angle to achieve an accurate ratio of intensities for the refinement (Supplemental Material [55]). Profile parameters including scaling, Gaussian, and Lorentzian terms, as well as the unit cell were initially refined.

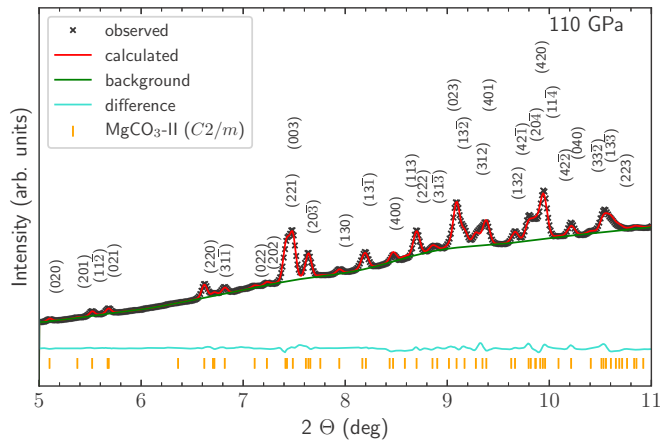


FIG. 6. Rietveld refinement of diffraction data collected at 110 GPa. The structural model by Oganov *et al.* [38] for  $\text{MgCO}_3\text{-II}$  ( $C2/m$  phase) was used for the refinement ( $\lambda = 0.2898 \text{ \AA}$ ). Refined structural parameters are listed in the Supplemental Material [55].

The background was manually fitted, using a Chebychev function with 20 terms. To reduce the number of parameters, we constrained the isotropic atomic displacement parameters to be the same for symmetrically independent atoms of the same chemical species. Further, we employed restraints on the atomic distances and refined the atomic positions. Refined lattice parameters were  $a = 8.117(4) \text{ \AA}$ ,  $b = 6.510(1) \text{ \AA}$ ,  $c = 6.911(2) \text{ \AA}$ ,  $\beta = 103.858(9)^\circ$ ,  $V = 354.64(5) \text{ \AA}^3$ . Our refined structural model is in excellent agreement with the structure of the  $C2/m$  phase reported by Oganov *et al.* [38] and lattice parameters are well in agreement with those from Le Bail refinements for the same pressure range as reported by Maeda *et al.* [9].

Raman spectra of  $\text{MgCO}_3$  (magnesite) and  $\text{MgCO}_3\text{-II}$  ( $C2/m$ -phase) were measured upon pressure release (Figs. 2 and 7). The pressure unexpectedly dropped during the first step of the release from 85 GPa down to 64 GPa. The pressure was then released in small steps down to ambient conditions, while Raman spectra were measured. During pressure release, the characteristic Raman bands of  $\text{MgCO}_3$  (magnesite) and those of  $\text{MgCO}_3\text{-II}$  ( $C2/m$  phase) could concomitantly be observed in the pressure range between 39.6–85 GPa. At lower pressures, only the  $A_{1g}(\nu_1)$  and  $E_g(\nu_4)$  modes of  $\text{MgCO}_3$  (magnesite) remained. The low-frequency  $E_g$  modes reappeared at around 5 GPa.  $\text{MgCO}_3$  (magnesite) was eventually recovered at ambient conditions, unequivocally showing that no decomposition occurred after laser heating at high pressures.

### C. Phase diagram of $\text{MgCO}_3$

Based on the results from this study in conjunction with data from the literature [9,26,31,32,40,70], we revise the phase diagram of  $\text{MgCO}_3$  (Fig. 8). A first phase diagram of  $\text{MgCO}_3$  was given by Isshiki *et al.* [26] in which phase boundaries were drawn for the magnesite to “magnesite-II” phase transition and the decomposition behavior of  $\text{MgCO}_3$ , determined by Fiquet *et al.* [31], was extended to higher  $P, T$  conditions. Another phase diagram at lower  $P, T$  conditions

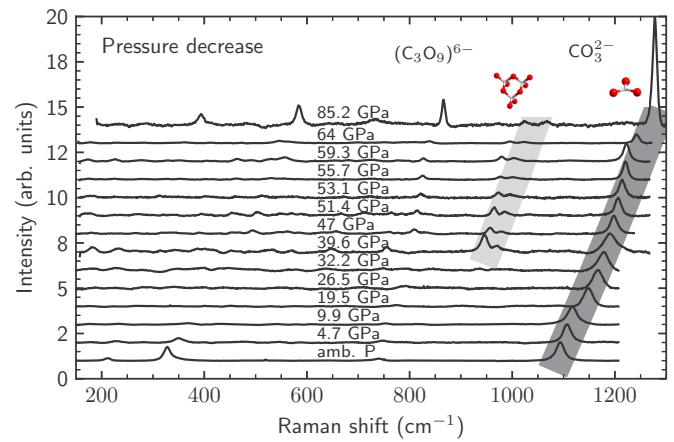


FIG. 7. Raman spectra of  $\text{MgCO}_3$  (magnesite) +  $\text{MgCO}_3\text{-II}$  ( $C2/m$ ) obtained during decompression down to ambient conditions. Frequencies of the  $(\text{C}_3\text{O}_9)^{6-}$  ring bending (light grey) are observed down to  $\sim 40$  GPa. The concomitant presence of a characteristic mode ( $\text{CO}_3^{2-}$ -stretching mode) of  $\text{MgCO}_3$  (magnesite) indicated in dark grey shows the coexistence of magnesite and metastable  $\text{MgCO}_3\text{-II}$ .  $\text{MgCO}_3$  (magnesite) is recovered at low pressures and ambient conditions.

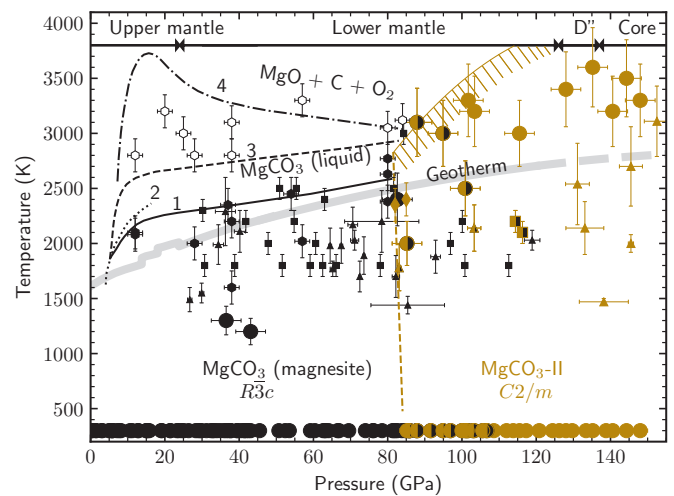


FIG. 8. Phase relations in the  $\text{MgCO}_3$  system with respect to the depth profile of the Earth’s mantle and outermost core. Markers correspond to studies, while colors denote distinct phases (black = magnesite, yellow =  $C2/m$  phase [38], white = magnesite +  $\text{MgO}$ ). Data from this study are shown as large circles and were obtained after temperature quenching at high pressures. Data obtained by Solopova *et al.* [32] are shown as hexagons, which have also been obtained after temperature quenching at high pressures. Squares, triangles, and diamonds correspond to the *in situ* data obtained in the studies by Isshiki *et al.* [26], Maeda *et al.* [9], and Boulard *et al.* [40], respectively. A typical mantle geotherm is shown as grey solid line [71]. The solid (1) and dashed (3) lines represent liquidus and decomposition for magnesite as reported by Solopova *et al.* [32]. The dotted line (2) represents the liquidus for magnesite as reported by Katsura and Ito [70]. The dash-dotted line (4) represents the decomposition of  $\text{MgCO}_3$  as reported by Fiquet *et al.* [31]. The dashed yellow line corresponds to the phase boundary of magnesite into the  $C2/m$ -phase derived here. The broad dashed yellow band presents a boundary above which we have not observed decomposition, but solid or liquid  $\text{MgCO}_3\text{-II}$ .

was reported by Solopova *et al.* [32], where the melting- and decomposition behavior of magnesite was described. The slope of the melting curve was discussed to be less steep than that reported by Katsura and Ito [70]. Also, for pressures below 50 GPa, the decomposition of  $\text{MgCO}_3$  (magnesite) was shown to happen at significantly lower temperatures than reported by Fiquet *et al.* [31], while at higher pressures both curves are approaching one another. We combined the contents of the phase diagrams from both studies [26,32] and added data points obtained in this study (large filled circles in Fig. 8) along with data points of the available high-pressure, high-temperature studies on  $\text{MgCO}_3$  beyond 50 GPa [9,26,32,40]. It should be borne in mind that our data and those by Solopova *et al.* [32] were obtained after temperature quenching and at high pressures, while all other data from the literature were measured *in situ* at high pressures and high temperatures [9,26,40].

In the present phase diagram, data points of  $\text{MgCO}_3$  (magnesite) are indicated by black circles (Fig. 8). According to Solopova *et al.* [32], our data points of heated  $\text{MgCO}_3$  (magnesite) fall within the conditions for magnesite as a solid phase. Our data points of  $\text{MgCO}_3$ -II (yellow circles) and  $\text{MgCO}_3$ -II associated with  $\text{MgCO}_3$  (black-yellow circles) are in very good agreement with the observations by Maeda *et al.* [9] and Boulard *et al.* [40]. Hence, we present the  $\text{MgCO}_3$ - $\text{MgCO}_3$ -II phase boundary (yellow dashed line) with a negative slope of  $dT/dP = -940 \text{ K GPa}^{-1}$  toward higher temperatures. Due to a lack of data, the phase boundary is only drawn up to the maximum available  $P, T$  conditions [40]. Our data points reveal that no decomposition is to be expected for  $\text{MgCO}_3$ -II at  $P, T$  conditions suggested by the decomposition lines of the previous phase diagrams [26,32] (see Supplemental Material [55]). As a consequence, the decomposition boundary of  $\text{MgCO}_3$ -II ( $C2/m$  phase) by Isshiki *et al.* [26] is not shown in the revised phase diagram (Fig. 8). Further,  $\text{MgCO}_3$  (magnesite) is observed to transform into  $\text{MgCO}_3$ -II rather than decomposing into  $\text{MgO} + \text{C} + \text{O}_2$  at pressures and temperatures above 85 GPa and  $\sim 3000 \text{ K}$ , respectively.

In our experiments, no other phase transition was found for pressures and temperatures up to 148 GPa and  $\sim 3600 \text{ K}$ . Our conclusion is consistent with the interpretation of Le Bail fits by Boulard *et al.* [40] and Maeda *et al.* [9] who conducted

*in situ* powder x-ray diffraction in the same  $P, T$  range. These combined observations suggest that the magnesite-II phase, found by Isshiki *et al.* [26], was very likely the  $C2/m$ -phase ( $\text{MgCO}_3$ -II).

#### IV. CONCLUSIONS

This study provides the first Raman spectra of pure  $\text{MgCO}_3$  at pressures and temperatures up to 148 GPa and 3600 K. Our spectra allowed the identification of  $\text{MgCO}_3$ -II-tetracarbonate and the location of the phase boundary between  $\text{MgCO}_3$  (magnesite) and  $\text{MgCO}_3$ -II ( $C2/m$  phase). Based on our observations from Raman spectroscopy, x-ray diffraction, and density functional theory calculations, we propose a revised phase diagram for  $\text{MgCO}_3$ . At  $P, T$  conditions of Earth's upper mantle and upper part of the lower mantle (e.g., pressures up to  $\sim 80 \text{ GPa}$  and temperatures up to  $\sim 2500 \text{ K}$ ),  $\text{MgCO}_3$  is stable as magnesite ( $R\bar{3}c$ ) [26,32]. At  $P, T$  conditions of Earth's lowermost mantle and outermost core (e.g., 85–148 GPa and at temperatures above 2500 K), the stable polymorph  $\text{MgCO}_3$ -II is a monoclinic  $C2/m$ -tetracarbonate as predicted by Oganov *et al.* [38]. In the present study, we observe that  $\text{MgCO}_3$ -II can exist on pressure release down to  $\sim 40 \text{ GPa}$ . This is similar to an earlier observation of the existence of  $\text{CaCO}_3$ -tetracarbonate on pressure release down to 57 GPa [45].

#### ACKNOWLEDGMENTS

The authors acknowledge funding by the Deutsche Forschungsgemeinschaft (DFG)-Germany (FOR2125/CarboPaT, BA4020, WI1232) and BMBF (05K16RFA). C.J.P. is supported by the Royal Society through a Royal Society Wolfson Research Merit Award and the EPSRC through Grant No. EP/P022596/1. S.S.L. acknowledges the support of the Helmholtz Young Investigators Group CLEAR (VH-NG-1325). The  $2n + 1$  Raman theorem in CASTEP was developed under Grant No. EP/I030107/1. DESY (Hamburg, Germany), a member of the Helmholtz Association (HGF), is acknowledged for the provision of experimental facilities. We would like to thank Hanns-Peter Liermann and his team for assistance in using beamline P02.2.

- 
- [1] R. Dasgupta and M. M. Hirschmann, The deep carbon cycle and melting in Earth's interior, *Earth Planet. Sci. Lett.* **298**, 1 (2010).
- [2] P. B. Kelemen and C. E. Manning, Reevaluating carbon fluxes in subduction zones, what goes down, mostly comes up, *Proc. Natl. Acad. Sci.* **112**, E3997 (2015).
- [3] T. Plank and C. H. Langmuir, The chemical composition of subducting sediment and its consequences for the crust and mantle, *Chem. Geol.* **145**, 325 (1998).
- [4] N. H. Sleep and K. Zahnle, Carbon dioxide cycling and implications for climate on ancient Earth, *J. Geophys. Res.: Planets* **106**, 1373 (2001).
- [5] P. Clift and P. Vannucchi, Controls on tectonic accretion versus erosion in subduction zones: Implications for the origin and recycling of the continental crust, *Rev. Geophys.* **42**, 2003RG000127 (2004).
- [6] P. D. Clift, A revised budget for Cenozoic sedimentary carbon subduction, *Rev. Geophys.* **55**, 97 (2017).
- [7] V. Stagno, Y. Tange, N. Miyajima, C. McCammon, T. Irifune, and D. Frost, The stability of magnesite in the transition zone and the lower mantle as function of oxygen fugacity, *Geophys. Res. Lett.* **38**, L19309 (2011).
- [8] Y. N. Palyanov, Y. V. Bataleva, A. G. Sokol, Y. M. Borzdov, I. N. Kupriyanov, V. N. Reutsky, and N. V. Sobolev, Mantle–

- slab interaction and redox mechanism of diamond formation, *Proc. Natl. Acad. Sci.* **110**, 20408 (2013).
- [9] F. Maeda, E. Ohtani, S. Kamada, T. Sakamaki, N. Hirao, and Y. Ohishi, Diamond formation in the deep lower mantle: A high-pressure reaction of  $\text{MgCO}_3$  and  $\text{SiO}_2$ , *Sci. Rep.* **7**, 40602 (2017).
- [10] S. M. Dorfman, J. Badro, F. Nabiei, V. B. Prakapenka, M. Cantoni, and P. Gillet, Carbonate stability in the reduced lower mantle, *Earth Planet. Sci. Lett.* **489**, 84 (2018).
- [11] H. Keppler, M. Wiedenbeck, and S. S. Shcheka, Carbon solubility in olivine and the mode of carbon storage in the Earth's mantle, *Nature* **424**, 414 (2003).
- [12] S. S. Shcheka, M. Wiedenbeck, D. J. Frost, and H. Keppler, Carbon solubility in mantle minerals, *Earth Planet. Sci. Lett.* **245**, 730 (2006).
- [13] M. Walter, G. Bulanova, L. Armstrong, S. Keshav, J. Blundy, G. Gudfinnsson, O. Lord, A. Lennie, S. Clark, C. Smith *et al.*, Primary carbonatite melt from deeply subducted oceanic crust, *Nature* **454**, 622 (2008).
- [14] K. F. Dziubek, M. Ende, D. Scelta, R. Bini, M. Mezouar, G. Garbarino, and R. Miletich, Crystalline polymeric carbon dioxide stable at megabar pressures, *Nat. Commun.* **9**, 3148 (2018).
- [15] D. J. Frost and C. A. McCammon, The redox state of Earth's mantle, *Annu. Rev. Earth Planet Sci.* **36**, 389 (2008).
- [16] R. Dasgupta, A. Buono, G. Whelan, and D. Walker, High-pressure melting relations in Fe–C–S systems: Implications for formation, evolution, and structure of metallic cores in planetary bodies, *Geochim. Cosmochim. Acta* **73**, 6678 (2009).
- [17] M. J. Walter, S. C. Kohn, D. Araujo, G. P. Bulanova, C. B. Smith, E. Gaillou, J. Wang, A. Steele, and S. B. Shirey, Deep mantle cycling of oceanic crust: Evidence from diamonds and their mineral inclusions, *Science* **334**, 54 (2011).
- [18] N. Martirosyan, T. Yoshino, A. Shatskiy, A. Chanyshev, and K. Litasov, The  $\text{CaCO}_3$ –Fe interaction: Kinetic approach for carbonate subduction to the deep Earth's mantle, *Phys. Earth Planet. Inter.* **259**, 1 (2016).
- [19] S. Goes, R. Agrusta, J. Van Hunen, and F. Garel, Subduction-transition zone interaction: A review, *Geosphere* **13**, 644 (2017).
- [20] T. R. McGetchin and J. Besancon, Carbonate inclusions in mantle-derived pyropes, *Earth Planet. Sci. Lett.* **18**, 408 (1973).
- [21] A. Wang, J. D. Pasteris, H. O. Meyer, and M. L. Dele-Duboi, Magnesite-bearing inclusion assemblage in natural diamond, *Earth Planet. Sci. Lett.* **141**, 293 (1996).
- [22] C.-T. Lee, R. L. Rudnick, W. F. McDonough, and I. Horn, Petrologic and geochemical investigation of carbonates in peridotite xenoliths from northeastern Tanzania, *Contrib. Mineral. Petrol.* **139**, 470 (2000).
- [23] F. E. Brenker, C. Vollmer, L. Vincze, B. Vekemans, A. Szymanski, K. Janssens, I. Szaloki, L. Nasdala, W. Joswig, and F. Kaminsky, Carbonates from the lower part of transition zone or even the lower mantle, *Earth Planet. Sci. Lett.* **260**, 1 (2007).
- [24] F. Kaminsky, Mineralogy of the lower mantle: A review of 'super-deep' mineral inclusions in diamond, *Earth-Sci. Rev.* **110**, 127 (2012).
- [25] F. V. Kaminsky, I. D. Ryabchikov, and R. Wirth, A primary natrocarbonatitic association in the Deep Earth, *Mineral. Petrol.* **110**, 387 (2016).
- [26] M. Isshiki, T. Irifune, K. Hirose, S. Ono, Y. Ohishi, T. Watanuki, E. Nishibori, M. Takata, and M. Sakata, Stability of magnesite and its high-pressure form in the lowermost mantle, *Nature* **427**, 60 (2004).
- [27] A. Rohrbach and M. W. Schmidt, Redox freezing and melting in the earth's deep mantle resulting from carbon–iron redox coupling, *Nature* **472**, 209 (2011).
- [28] L. Bayarjargal, C.-J. Fruhner, N. Schrodtr, and B. Winkler,  $\text{CaCO}_3$  phase diagram studied with Raman spectroscopy at pressures up to 50 GPa and high temperatures and DFT modeling, *Phys. Earth Planet. Inter.* **281**, 31 (2018).
- [29] J. Binck, S. Chariton, M. Stekiel, L. Bayarjargal, W. Morgenroth, V. Milman, L. Dubrovinsky, and B. Winkler, High-pressure, high-temperature phase stability of iron-poor dolomite and the structures of dolomite-IIIc and dolomite-V, *Phys. Earth Planet. Inter.* **299**, 106403 (2020).
- [30] V. Cerantola, E. Bykova, I. Kuppenko, M. Merlini, L. Ismailova, C. McCammon, M. Bykov, A. I. Chumakov, S. Petitgirard, I. Kantor, V. Svitlyk, J. Jacobs, M. Hanfland, M. Mezouar, C. Prescher, R. Rüffer, V. B. Prakapenka, and L. Dubrovinsky, Stability of iron-bearing carbonates in the deep Earth's interior, *Nat. Commun.* **8**, 15960 (2017).
- [31] G. Fiquet, F. Guyot, M. Kunz, J. Matas, D. Andrault, and M. Hanfland, Structural refinements of magnesite at very high pressure, *Am. Mineralogist* **87**, 1261 (2002).
- [32] N. Solopova, L. Dubrovinsky, A. Spivak, Y. A. Litvin, and N. Dubrovinskaia, Melting and decomposition of  $\text{MgCO}_3$  at pressures up to 84 GPa, *Phys. Chem. Miner.* **42**, 73 (2015).
- [33] X. Yao, C. Xie, X. Dong, A. R. Oganov, and Q. Zeng, Novel high-pressure calcium carbonates, *Phys. Rev. B* **98**, 014108 (2018).
- [34] S. S. Santos, M. L. Marcondes, J. F. Justo, and L. V. Assali, Stability of calcium and magnesium carbonates at Earth's lower mantle thermodynamic conditions, *Earth Planet. Sci. Lett.* **506**, 1 (2019).
- [35] N. V. Skorodumova, A. B. Belonoshko, L. Huang, R. Ahuja, and B. Johansson, Stability of the  $\text{MgCO}_3$  structures under lower mantle conditions, *Am. Mineral.* **90**, 1008 (2005).
- [36] S. Arapan, J. Souza de Almeida, and R. Ahuja, Formation of  $sp^3$  Hybridized Bonds and Stability of  $\text{CaCO}_3$  at Very High Pressure, *Phys. Rev. Lett.* **98**, 268501 (2007).
- [37] A. R. Oganov, C. W. Glass, and S. Ono, High-pressure phases of  $\text{CaCO}_3$ : Crystal structure prediction and experiment, *Earth Planet. Sci. Lett.* **241**, 95 (2006).
- [38] A. R. Oganov, S. Ono, Y. Ma, C. W. Glass, and A. Garcia, Novel high-pressure structures of  $\text{MgCO}_3$ ,  $\text{CaCO}_3$  and  $\text{CO}_2$  and their role in Earth's lower mantle, *Earth Planet. Sci. Lett.* **273**, 38 (2008).
- [39] C. J. Pickard and R. J. Needs, Structures and stability of calcium and magnesium carbonates at mantle pressures, *Phys. Rev. B* **91**, 104101 (2015).
- [40] E. Boulard, A. Gloter, A. Corgne, D. Antonangeli, A.-L. Auzende, J.-P. Perrillat, F. Guyot, and G. Fiquet, New host for carbon in the deep Earth, *Proc. Natl. Acad. Sci.* **108**, 5184 (2011).
- [41] E. Boulard, N. Menguy, A. L. Auzende, K. Benzerara, H. Bureau, D. Antonangeli, A. Corgne, G. Morard, J. Siebert, J. P. Perrillat, F. Guyot, and G. Fiquet, Experimental investigation of the stability of Fe-rich carbonates in the lower mantle, *J. Geophys. Res.: Solid Earth* **117**, B02208 (2012).

- [42] E. Boulard, D. Pan, G. Galli, Z. Liu, and W. L. Mao, Tetrahedrally coordinated carbonates in Earth's lower mantle, *Nat. Commun.* **6**, 6311 (2015).
- [43] M. Merlini, M. Hanfland, A. Salamat, S. Petitgirard, and H. Müller, The crystal structures of  $\text{Mg}_2\text{Fe}_2\text{C}_4\text{O}_{13}$ , with tetrahedrally coordinated carbon, and  $\text{Fe}_{13}\text{O}_{19}$ , synthesized at deep mantle conditions, *Am. Mineral.* **100**, 2001 (2015).
- [44] M. Merlini, V. Cerantola, G. D. Gatta, M. Gemmi, M. Hanfland, I. Kupenko, P. Lotti, H. Müller, and L. Zhang, Dolomite-IV: Candidate structure for a carbonate in the Earth's lower mantle, *Am. Mineral.* **102**, 1763 (2017).
- [45] S. S. Lobanov, X. Dong, N. S. Martirosyan, A. I. Samtsevich, V. Stevanovic, P. N. Gavryushkin, K. D. Litasov, E. Greenberg, V. B. Prakapenka, A. R. Oganov *et al.*, Raman spectroscopy and x-ray diffraction of  $sp^3$   $\text{CaCO}_3$  at lower mantle pressures, *Phys. Rev. B* **96**, 104101 (2017).
- [46] S. Chariton, M. Bykov, E. Bykova, E. Koemets, T. Fedotenko, B. Winkler, M. Hanfland, V. B. Prakapenka, E. Greenberg, C. McCammon, and L. Dubrovinsky, The crystal structures of Fe-bearing  $\text{MgCO}_3$   $sp^2$ - and  $sp^3$ -carbonates at 98 GPa from single-crystal X-ray diffraction using synchrotron radiation, *Acta Cryst. E* **76**, 715 (2020).
- [47] A. Spivak, N. Solopova, V. Cerantola, E. Bykova, E. Zakharchenko, L. Dubrovinsky, and Y. Litvin, Raman study of  $\text{MgCO}_3$ - $\text{FeCO}_3$  carbonate solid solution at high pressures up to 55 GPa, *Phys. Chem. Miner.* **41**, 633 (2014).
- [48] I. Efthimiopoulos, S. Jahn, A. Kuras, U. Schade, and M. Koch-Müller, Combined high-pressure and high-temperature vibrational studies of dolomite: Phase diagram and evidence of a new distorted modification, *Phys. Chem. Miner.* **44**, 465 (2017).
- [49] C. E. Vennari and Q. Williams, A novel carbon bonding environment in deep mantle high-pressure dolomite, *Am. Mineral.* **103**, 171 (2018).
- [50] Q. Williams, B. Collerson, and E. Knittle, Vibrational spectra of magnesite ( $\text{MgCO}_3$ ) and calcite-III at high pressures, *Am. Mineral.* **77**, 1158 (1992).
- [51] P. Gillet, Stability of magnesite ( $\text{MgCO}_3$ ) at mantle pressure and temperature conditions: A Raman spectroscopic study, *Am. Mineral.* **78**, 1328 (1993).
- [52] S. Ni, T. Li, and X. Yang, Hydrothermal synthesis of  $\text{MgCO}_3$  and its optical properties, *J. Alloys Compd.* **509**, 7874 (2011).
- [53] B. H. Toby and R. B. Von Dreele, *GSAS-II*: The genesis of a modern open-source all purpose crystallography software package, *J. Appl. Crystallogr.* **46**, 544 (2013).
- [54] S. Göttlicher and A. Vegas, Electron-density distribution in magnesite ( $\text{MgCO}_3$ ), *Acta Crystallogr. Sect. B* **44**, 362 (1988).
- [55] See Supplemental Material at <http://link.aps.org/supplemental/10.1103/PhysRevMaterials.4.055001> for additional Raman and x-ray diffraction data, a description of pseudopotentials and a modified phase diagram.
- [56] R. Boehler, New diamond cell for single-crystal X-ray diffraction, *Rev. Sci. Instrum.* **77**, 115103 (2006).
- [57] H. Mao, P. Bell, J. t. Shaner, and D. Steinberg, Specific volume measurements of Cu, Mo, Pd, and Ag and calibration of the ruby R1 fluorescence pressure gauge from 0.06 to 1 Mbar, *J. Appl. Phys.* **49**, 3276 (1978).
- [58] H. Mao, J.-A. Xu, and P. Bell, Calibration of the ruby pressure gauge to 800 kbar under quasi-hydrostatic conditions, *J. Geophys. Res.: Solid Earth* **91**, 4673 (1986).
- [59] Y. Akahama and H. Kawamura, Pressure calibration of diamond anvil Raman gauge to 310 GPa, *J. Appl. Phys.* **100**, 043516 (2006).
- [60] A. Dewaele, P. Loubeyre, and M. Mezouar, Equations of state of six metals above 94 GPa, *Phys. Rev. B* **70**, 094112 (2004).
- [61] L. R. Benedetti and P. Loubeyre, Temperature gradients, wavelength-dependent emissivity, and accuracy of high and very-high temperatures measured in the laser-heated diamond cell, *High Press. Res.* **24**, 423 (2004).
- [62] C. Prescher and V. B. Prakapenka, DIOPTAS: A program for reduction of two-dimensional X-ray diffraction data and data exploration, *High Press. Res.* **35**, 223 (2015).
- [63] S. J. Clark, M. D. Segall, C. J. Pickard, P. J. Hasnip, M. I. Probert, K. Refson, and M. C. Payne, First principles methods using CASTEP, *Z. Kristallogr.* **220**, 567 (2005).
- [64] K. Lejaeghere, G. Bihlmayer, T. Björkman, P. Blaha, S. Blügel, V. Blum, D. Caliste, I. E. Castelli, S. J. Clark, A. Dal Corso *et al.*, Reproducibility in density functional theory calculations of solids, *Science* **351**, aad3000 (2016).
- [65] J. P. Perdew, K. Burke, and M. Ernzerhof, Generalized Gradient Approximation Made Simple, *Phys. Rev. Lett.* **77**, 3865 (1996).
- [66] H. J. Monkhorst and J. D. Pack, Special points for Brillouin-zone integrations, *Phys. Rev. B* **13**, 5188 (1976).
- [67] K. Miwa, Prediction of raman spectra with ultrasoft pseudopotentials, *Phys. Rev. B* **84**, 094304 (2011).
- [68] H. Rutt and J. Nicola, Raman spectra of carbonates of calcite structure, *J. Phys. C* **7**, 4522 (1974).
- [69] W. D. Bischoff, S. K. Sharma, and F. T. MacKenzie, Carbonate ion disorder in synthetic and biogenic magnesian calcites: A Raman spectral study, *Am. Mineral.* **70**, 581 (1985).
- [70] T. Katsura and E. Ito, Melting and subsolidus phase relations in the  $\text{MgSiO}_3$ - $\text{MgCO}_3$  system at high pressures: Implications to evolution of the Earth's atmosphere, *Earth Planet. Sci. Lett.* **99**, 110 (1990).
- [71] T. Katsura, A. Yoneda, D. Yamazaki, T. Yoshino, and E. Ito, Adiabatic temperature profile in the mantle, *Phys. Earth Planet. Inter.* **183**, 212 (2010).